Supporting information for

Atmospheric gaseous hydrochloric and hydrobromic acid in urban Beijing, China: detection, source identification and potential atmospheric impacts

Xiaolong Fan[1#], Jing Cai[2#], Chao Yan[2], Jian Zhao[2], Yishuo Guo[1], Chang Li[1], Kaspar R. Dällenbach[2], Feixue Zheng[1], Zhuohui Lin[1], Biwu Chu[3,4], Yonghong Wang[2], Lubna Dada[2], Qiaozhi Zha[2], Wei Du[2], Jenni Kontkanen[2], Theo Kurtén[5], Siddhart Iyer[6], Joni T Kujansuu[1,2], Tuukka Petäjä[2], Douglas R. Worsnop[7], Veli-Matti Kerminen[2],Yongchun Liu[1], Federico Bianchi[2], Yee Jun Tham[2]*, Lei Yao[2]*, Markku Kulmala[1,2,8]

Affiliations:

[1]Aerosol and Haze Laboratory, Beijing Advanced Innovation Center for Soft Matter Science and Engineering, Beijing University of Chemical Technology, Beijing 100089, China

[2] Institute for Atmospheric and Earth System Research / Physics, Faculty of Science, University of Helsinki 00560, Finland

[3] State Key Joint Laboratory of Environment Simulation and Pollution Control, Research Center for Eco-Environmental Sciences, Chinese Academy of Sciences, Beijing 100085, China

[4] Center for Excellence in Regional Atmospheric Environment, Institute of Urban Environment, Chinese Academy of Sciences, Xiamen 361021, China

[5] Department of Chemistry, University of Helsinki, FI-00014 Helsinki, Finland

[6] Aerosol Physics Laboratory, Physics Unit, Tampere University, Tampere 33100, Finland

[7] Aerodyne Research Inc., Billerica, Massachusetts 01821, USA

[8] Joint International Research Laboratory of Atmospheric and Earth System Sciences (JirLATEST), Nanjing University, Nanjing 210023, China.

[#] These authors contributed equally.

Correspondence: Lei Yao (lei.yao@helsinki.fi) and Yee Jun Tham (yee.tham@helsinki.fi)

Section S1. ACSM, MARGA and Aethalometer

Table S1. Instruments

	Phase	
	Gas	Particulate
CI-APi-LTOF	√	×
ACSM	×	√
MARGA	√	√
Aethalometer (AE33)	×	√

ACSM

An online Time-of-Flight-Aerosol Chemical Speciation Monitor (ToF-ACSM, Aerodyne Research Inc., US, hereafter ACSM) was deployed to measure nitrate, sulphate, ammonium, chloride and organic at the same site with a $PM_{2.5}$ aerodynamic lens and standard vaporizer. Particles first went through a $PM_{2.5}$ cyclone and then a 3-m steel tube before being analyzed by ToF-ACSM. The ionization efficiency (IE) and relative ionization efficiency (RIE) of Cl were obtained by calibrations with pure standards of ammonium nitrate and ammonium chloride. It should be noted that the Cl measured by ACSM was non-refractory chloride compounds such as ammonium chloride. Yet, a high correlation was observed between Cl measured by aerosol mass spectrometry and automated ion chromatography method such as particle into liquid sampler (PILS), which measured total water soluble Cl in previous studies (Canagaratna et al., 2007). It suggested that the non-refractory Cl measured by ACSM could explain large proportion of particulate Cl in the urban environment. In addition, the contribution of crustal materials was relatively low during the winter season (He et al., 2001; Yu et al., 2013), further supporting that its contribution to refractory Cl should be minor during our sampling period.

MARGA

The Monitor for AeRosols and Gases (MARGA, Metrohm AG Inc., Switzerland) is an online analyzer that semi-continuously measures water-soluble gases (i.e. HCl, HONO, HNO_3, SO_2, NH_3) and chemical composition of aerosols (i.e. Cl^-, NO_3^-, SO_4^{2-}, Na^+, NH_4^+, K^+, Mg^{2+}, Ca^{2+}) at an hourly temporal resolution using ion chromatography. The ambient sample containing gaseous species and $PM_{2.5}$ particles passes through a wet rotating denuder (WRD). WRD has two concentric glass cylinders coated with absorption solution (H_2O_2), which causes the gas diffuse into aqueous film (Keuken et al., 1988; Otjes et al., 1993; Rumsey et al., 2011). The samples are analyzed by using cation and anion ion conductivity detectors (IC, Metrohm AG Inc., Switzerland). The analytical accuracy was controlled by internal standard LiBr, which is injected simultaneously and then mixed with the sample. In addition, to verify the accuracy of HCl concentration, an external standard test was conducted by replacing the absorption solution with a known liquid anion standard containing Cl^- (sigma-aldrich, multielement ion chromatography anion standard solution, containing F^-, Cl^-, NO_3^-, PO_4^{3-}, SO_4^{2-}) every week.

Aethalometer (AE33)

Black carbon (BC) mass concentrations were measured by the aethalometer (Model AE33, Magee Scientific Inc., USA). Particles first went through a $PM_{2.5}$ cyclone and the aerosol sample were collected continuously through spots on the filter tape. Two measurements are obtained from the loaded and unloaded spot, which from same air stream, with different rates of accumulation of the aerosol sample. The transmission of light was measured at 7 different wavelengths. AE33 calculates the instantaneous concentration of optically absorbing aerosols from the rate of change of the attenuation of light

transmitted through the particle-laden filter (Drinovec et al., 2014) and then provide the compensated particle light absorption and BC concentration. In this study, aerosol particles are continually sampled on filter and the optical attenuation is measured with high time resolution.

Section S2. A typical raw mass spectrum and high-resolution peak fittings of interested compounds

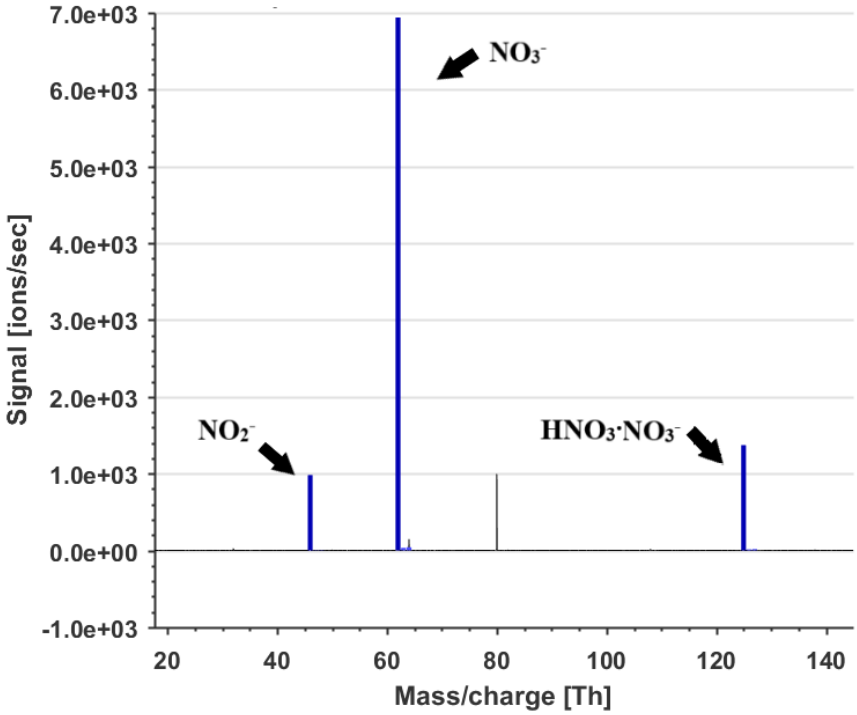

Figure S1. Reagent ions signal of NO_2^-, NO_3^- and $HNO_3 \cdot NO_3^-$.

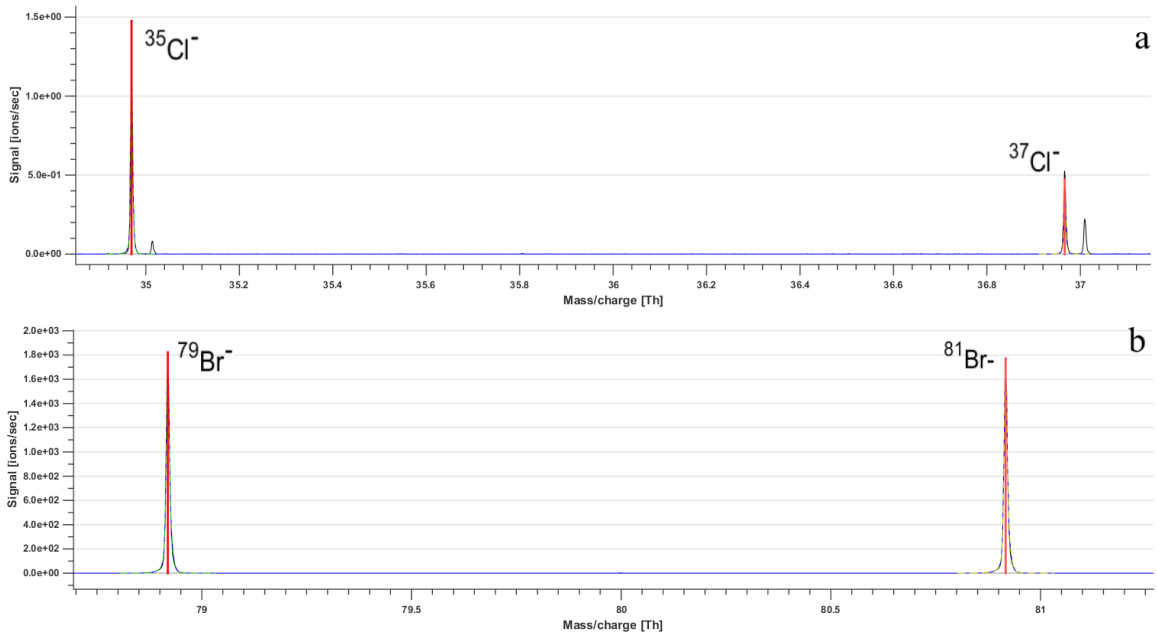

Figure S2. (a) High resolution peak fitting of $^{35}Cl^-$ and $^{37}Cl^-$, which has the same ratio ($^{35}Cl^-$:$^{37}Cl^-$ = 3:1) as isotopic abundances of the chlorine elements; (b) High resolution peak fitting of ^{79}Br and $^{81}Br^-$, which has the same ratio ($^{79}Br^-$:$^{81}Br^-$ = 1:1) as isotopic abundances of the bromine elements.

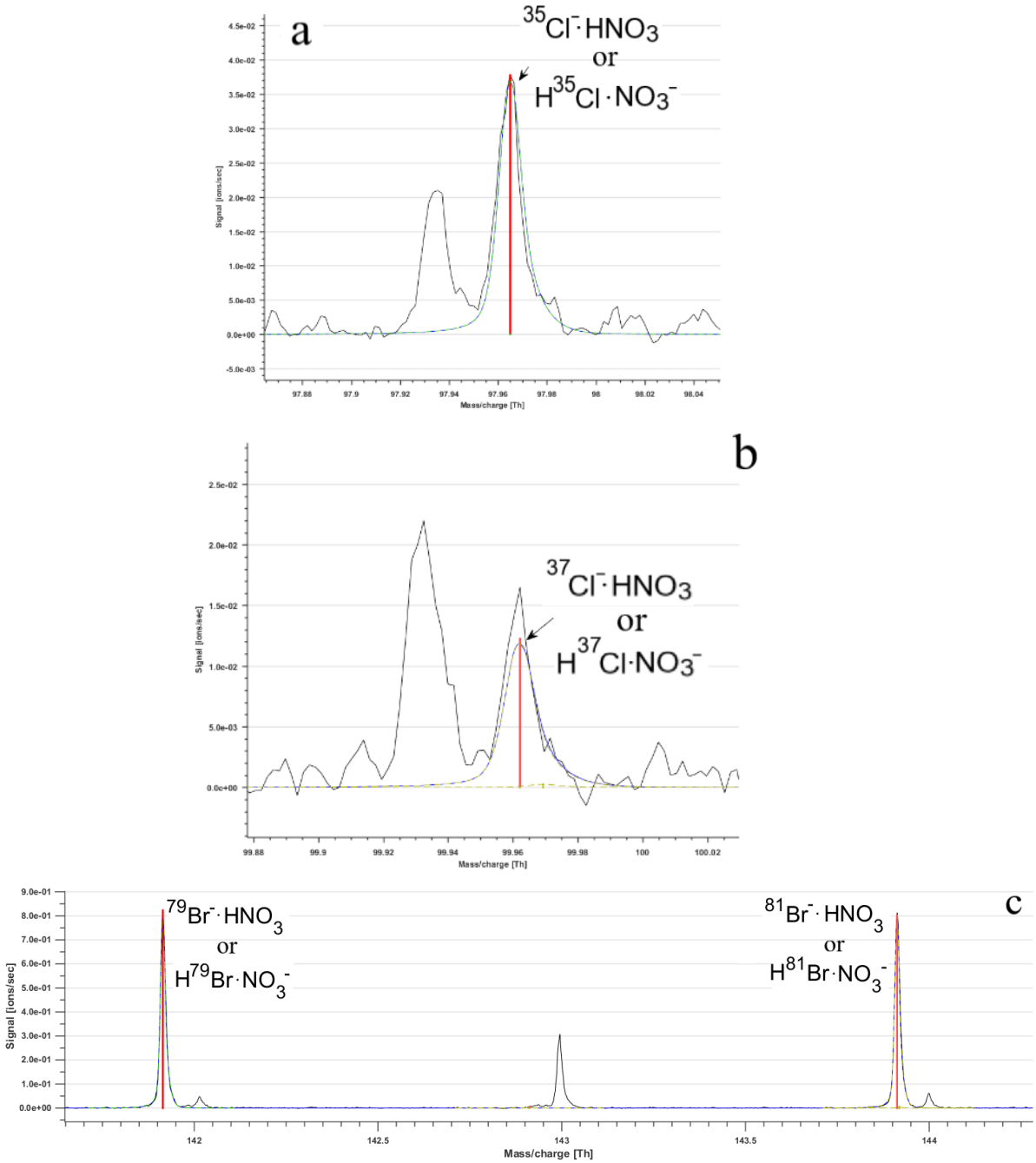

Figure S3. High resolution peak fitting of $^{35}Cl^{-}\cdot HNO_3$ (or $H^{35}Cl\cdot NO_3^{-}$) (a), $^{37}Cl^{-}\cdot HNO_3$ (or $H^{37}Cl\cdot NO_3^{-}$) (b), $^{79}Br^{-}\cdot HNO_3$ (or $H^{79}Br\cdot NO_3^{-}$) and $^{81}Br^{-}\cdot HNO_3$ (or $H^{81}Br\cdot NO_3^{-}$) (c).

Section S3. Cluster stabilities

Initial geometries of molecules were generated by performing a molecular mechanics (MMFF) conformer sampling using the Spartan 18' program (Benson et al., 2008). All molecules and clusters studied here had only one possible conformer geometry. The molecules were optimized using density functional methods at the ωB97X-D/aug-cc-pVTZ level (ωB97X-D/aug-cc-pVTZ-PP for bromide containing molecules) and ultrafine integration grid with the Gaussian 16 program(Yu et al., 2017). Bromide pseudopotential definitions were taken from EMSL basis set library (Wang et al., 2017; Wilson et al., 1999). Single-point calculations on the optimized geometries were carried out at the DLPNO-CCSD(T)/def2-QZVPP level using the ORCA program version 4.0.0.2 (Neese, 2012; Riplinger and Neese, 2013) to provide the accurate final energies used to calculate the cluster binding enthalpies. The predicted sensitivities were derived by inputting the calculated binding enthalpies into the model presented in Iyer et al. (Iyer et al., 2016).

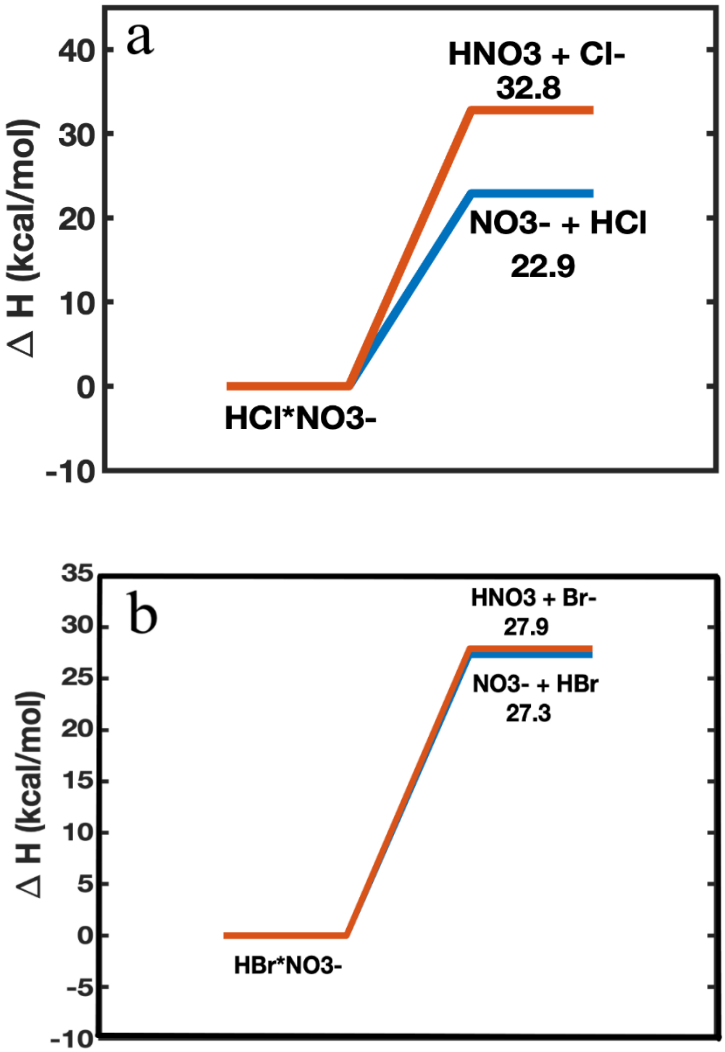

Figure S4. (a) The enthalpy of $HCl{\cdot}NO_3^-$ formed by HNO_3+Cl^- and NO_3^-+HCl and (b) the enthalpy of $HBr{\cdot}NO_3^-$ formed by HNO_3+Br^- and NO_3^-+HBr calculated at the DLPNO-CCSD(T)/def2-QZVPP// ωB97X-D/aug-cc-pVTZ-PP level of theory.

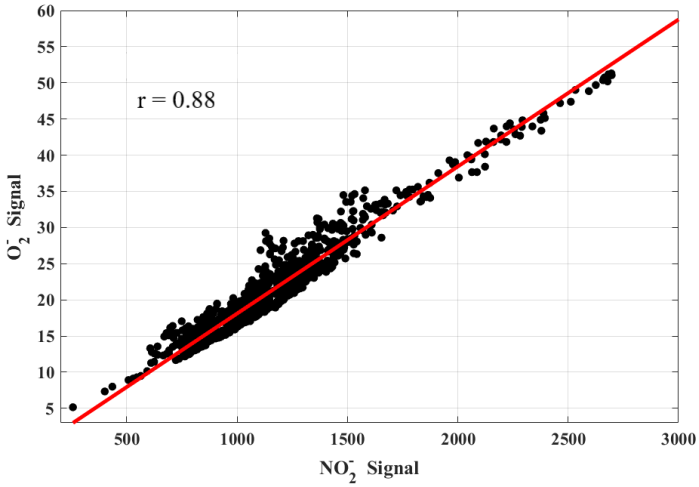

Figure S5. Excellent correlation (r = 0.88) between NO_2^- concentrations and O_2^- (with 1095 valid data) during observation periods.

Section S4. Laboratory experiment of HCl and HBr observation

In order to quantitively confirm HCl and HBr can be detected by CI-APi-LTOF, 1 ml liquid standard HCl (Gaosheng, 36%) and HBr (Macklin, 48%) were diluted in 1000 ml MILLIPORE® ultrapure water, respectively, which correspond to 1.2×10^{-2} mol L^{-1} HCl and 8.6×10^{-3} mol L^{-1} HBr. Then, 10 ml diluted HCl and HBr were mixed as sample and evaporated sample flow was carried by zero air at 1L min^{-1} into CI-APi-LTOF controlled by switch valve shown as Figure S6. After the injection of gaseous HCl and HBr, the signals of Cl^-, Br^-, $Cl^-\cdot HNO_3$ (or $HCl\cdot NO_3^-$) and $Br^-\cdot HNO_3$ (or $HCl\cdot NO_3^-$) started to increase (Figure S7), confirming that the HCl and HBr can be detected as Cl^-, Br^-, $Cl^-\cdot HNO_3$ (or $HCl\cdot NO_3^-$) and $Br^-\cdot HNO_3$ (or $HBr\cdot NO_3^-$) in CI-APi-LTOF.

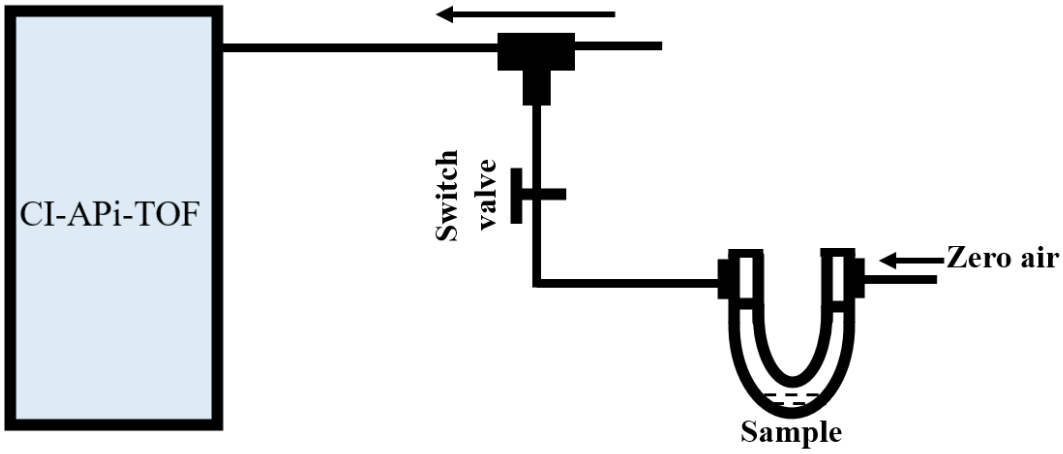

Figure S6. Schematic of experiment set up.

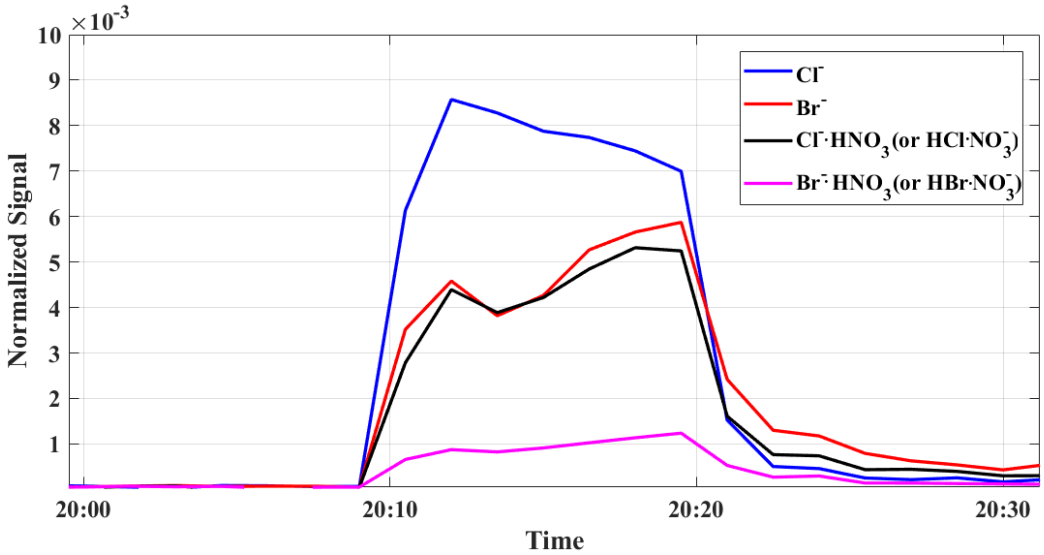

Figure S7. Cl^-, Br^-, $Cl^-\cdot HNO_3$ (or $HCl\cdot NO_3^-$) and $Br^-\cdot HNO_3$ (or $HBr\cdot NO_3^-$) signal measured by CI-APi-LTOF.

Section S5. Calibration factor

The HCl and HBr were measured by a NO_2^--based chemical ionization long time-of-flight mass spectrometer (CI-APi-LTOF). Direct calibrations for HCl and HBr were not available. In order to calibrate HCl concentration, we adopt the ambient HCl concentrations measured by MARGA for about 4 days (02.09.2019 to 06.09.2019) to indirectly calibrate the CI-APi-LTOF. Time profile of HCl concentration from MARGA and normalized signals of HCl by sum of NO_2^- and O_2^- ion from CI-APi-LTOF was depicted in Figure S8. From Figure S8a, it shows similar variation of the data from two different instruments and then plotting HCl concentration measured by MARGA versus HCl normalized signal measured by CI-APi-LTOF shown in Figure S8b. Data from MARGA correlates well with HCl normalized signal (r = 0.73). Thus, the obtained calibration factor for HCl is 2.84×10^{12} cm^{-3}.

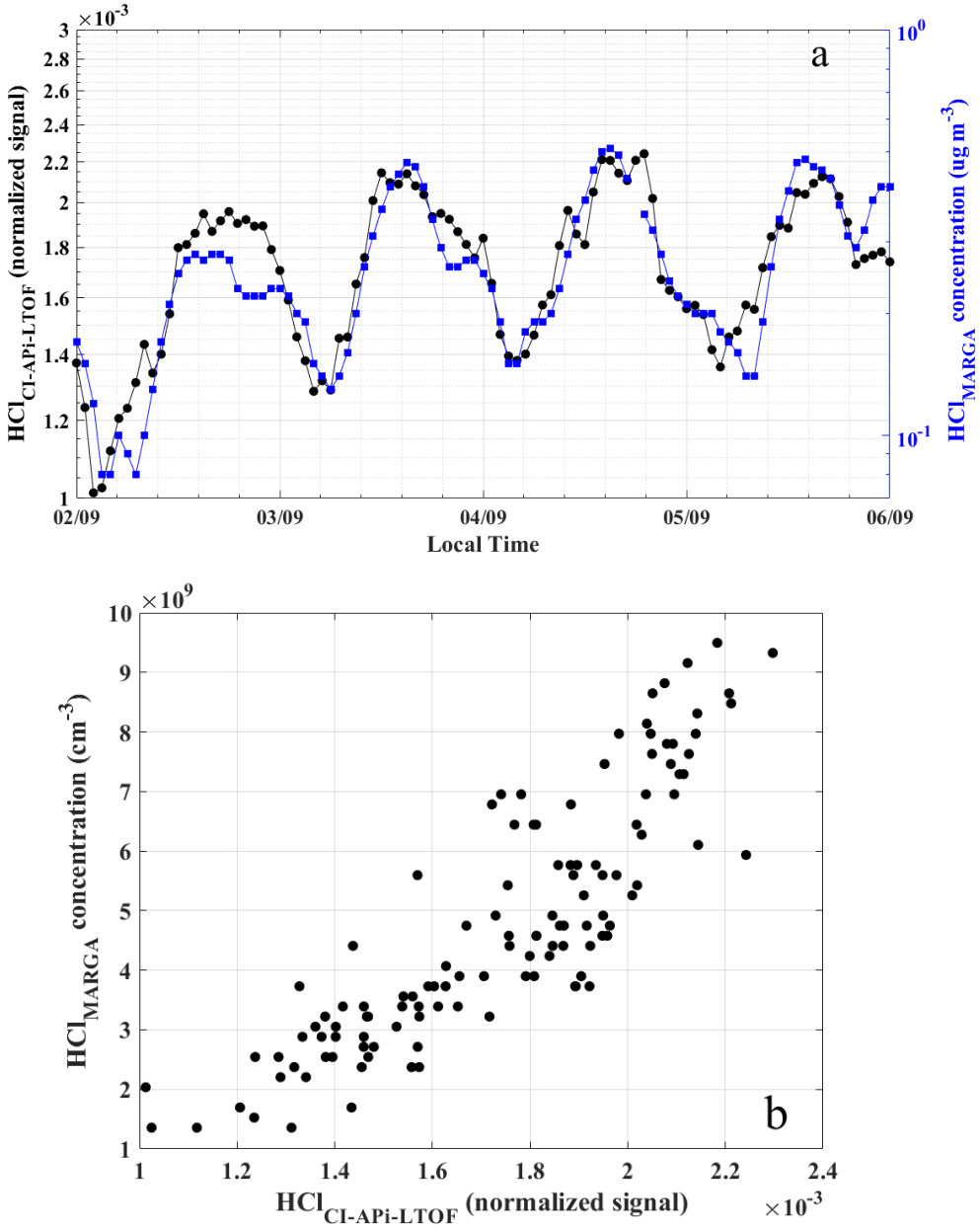

Figure S8. (a) Time series of normalized HCl signal measured by CI-APi-LTOF and HCl concentration measured by MARGA during calibration period and (b) Correlation (r = 0.73) between HCl concentration measured by MARGA and normalized HCl signals measured by CI-APi-LTOF.

Section S6. The effects of atmospheric temperature and the abundance of gaseous HNO_3 on HCl and HBr concentrations.

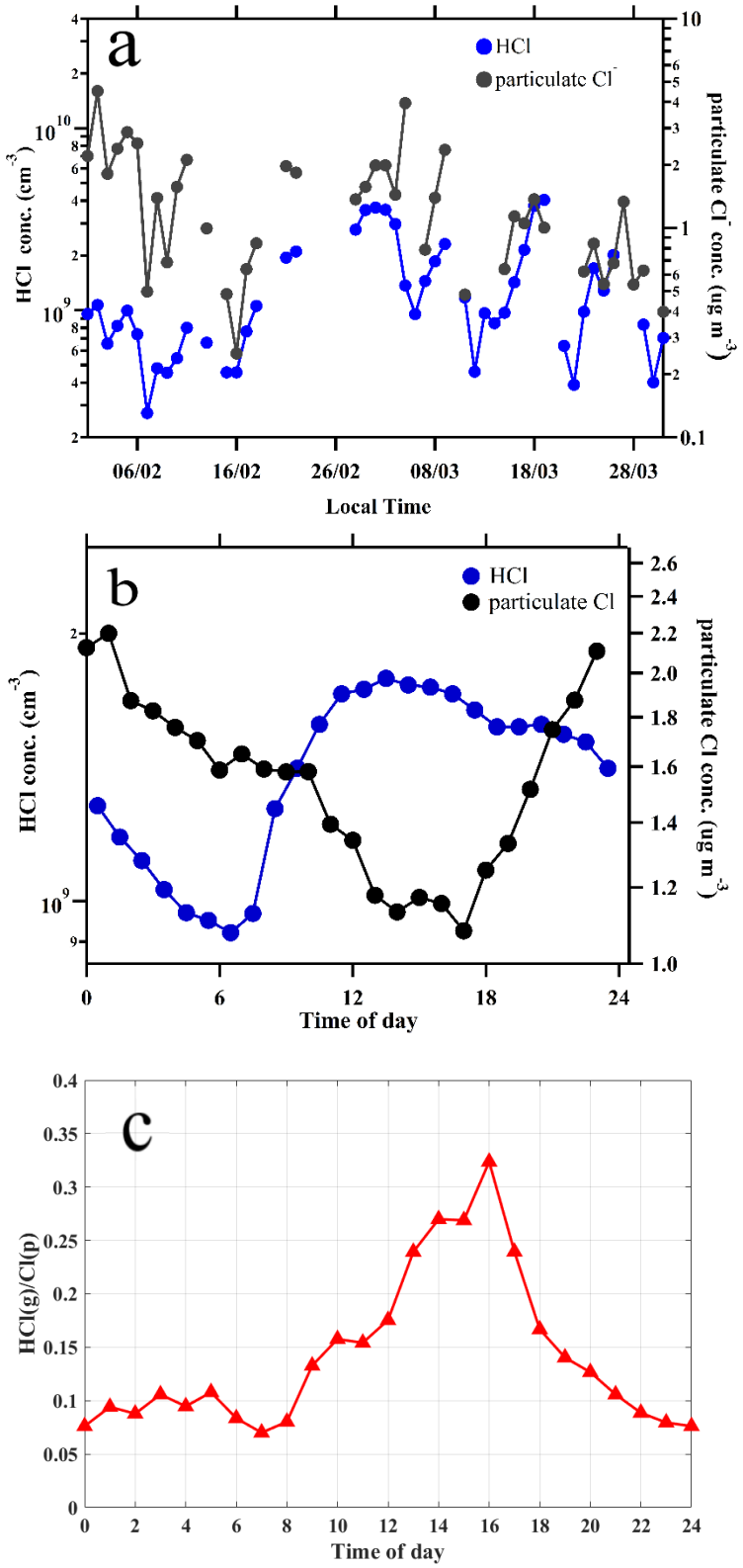

Figure S9. (a) Daily mean concentration of particulate chlorine and gaseous HCl, (b) Diurnal variation of HCl and particulate Cl concentration and (c) Diurnal variation of chloride gas to particle ratio.

Section S7. Source identification

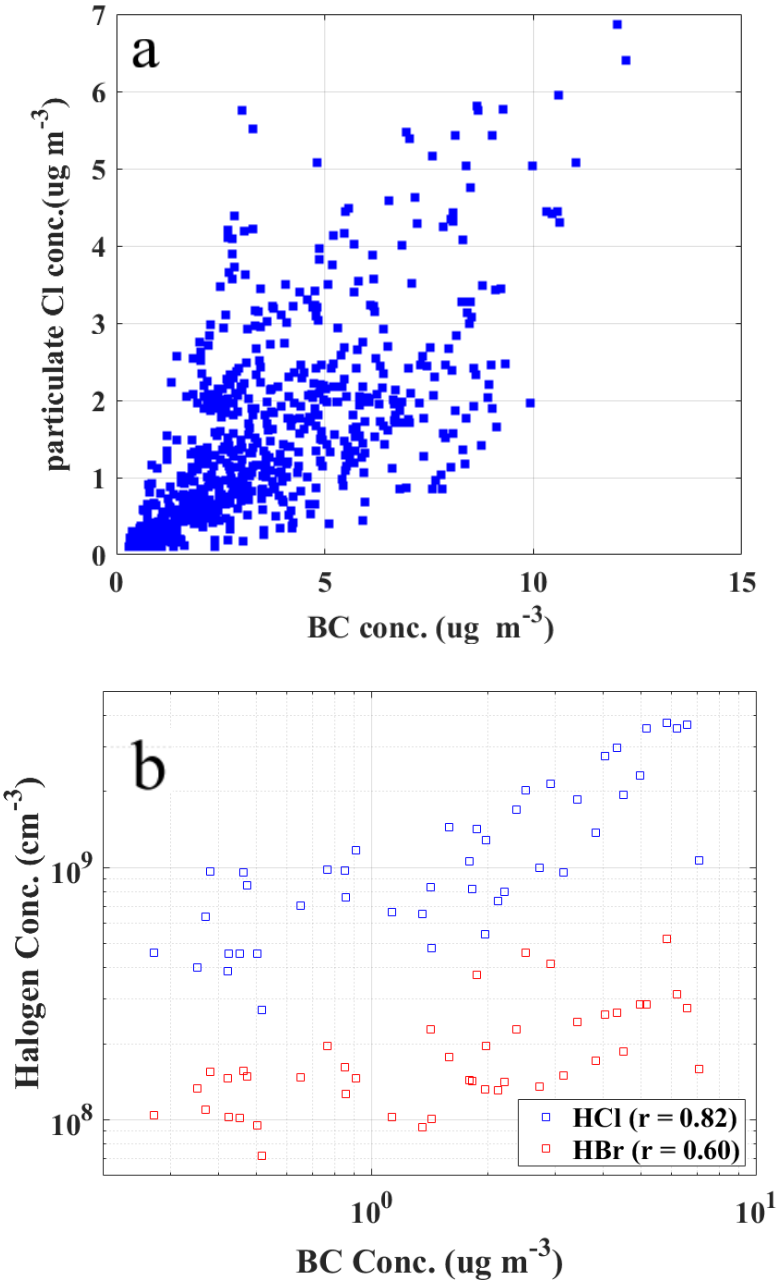

Figure S10. (a) Good correlation (*r* = 0.67) between hourly mean particulate Cl concentrations and black carbon (BC); (b) Correlations between HCl (*r* = 0.82), HBr (*r* = 0.60) daily mean concentrations and BC during observation periods from 1st Feb to 31st March, 2019.

Section S8. The calculations of OH concentration and production rate of atomic Cl and Br.

OH concentration:

In this work, there are no direct measurement of J_{NO2} and no direct measurement of OH radical concentration during observation periods. As shown in Figure S11a, the model well predicted (r = 0.97) the J_{NO2} from 21st May to 10th June, 2019. Then the J_{NO2} during this study was predicted using model. According to Xu et al. (Xu et al., 2015) estimated the OH radical concentration considering both photolysis rate (J_{O1D} and J_{NO_2}) and NO_2 concentration (C_{NO_2}) based on formula E(1).

$$c_{OH} = \frac{4.1\times10^{9}\times(JO1D)^{0.83}\times(JNO_2)^{0.19}\times(140c_{NO_2}+1)}{0.41c_{NO_2}^{2}+1.7c_{NO_2}+1} \quad \text{E(1)}$$

While in winter and spring, Beijing, it has been found that the OH radical concentration is linearly correlated with photolysis of ozone (Liu et al., 2020; Tan et al., 2019) (J_{O1D}), [OH] = $J_{O1D}\times2\times10^{11}$ molecules cm^{-3}, which the estimated OH concentrations were comparable according to equation E(1) shown in Figure S11b. Thus, OH radical concentration has been used based on the calculation results by Tan et al (2018) in this study.

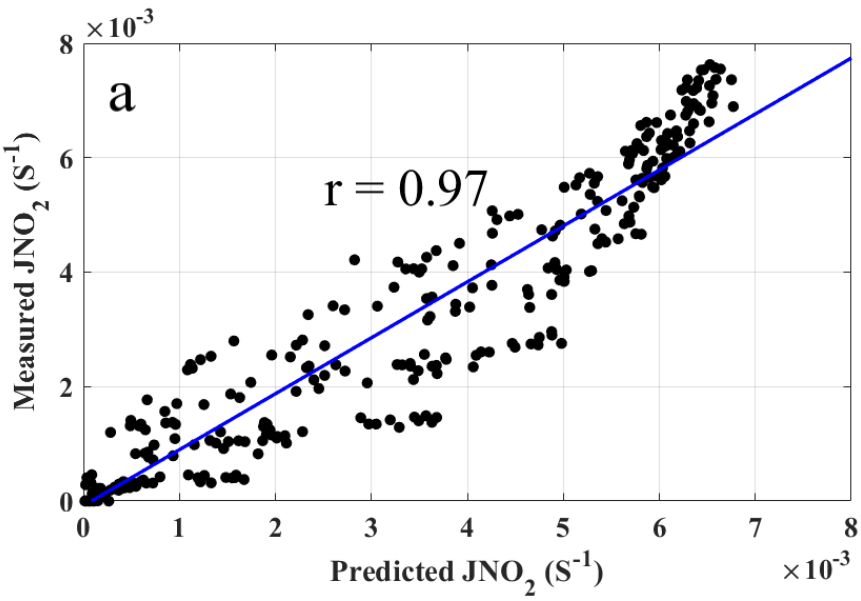

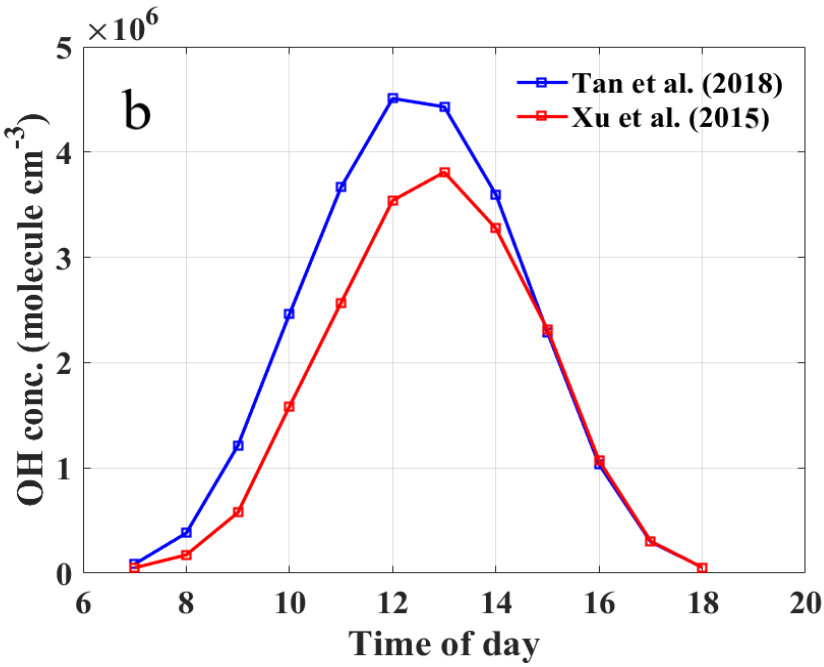

Figure S11. (a) Excellent correlation (r = 0.97) between measured and predicted JNO_2 from 21 May to 10 June, 2019; (b) Calculated diurnal curve of OH concentration based on Tan et al., (2018) and Xu et al., (2017) from 1 February to 31 March, 2019.

Production rates of atomic Cl and Br:

In order to determine the impacts of gas particle partitioning of HCl and HBr on atmospheric oxidation capacity and particulate chloride and bromine, an accurate measurement of gas phase HCl and HBr are required to assess the production rate of Cl and Br atoms via direct OH oxidation of HCl and HBr. The Cl· and Br· can be formed via the reactions (R (S1) and R (S2)) of HCl and HBr with OH.

$$HO + HCl \rightarrow H_2O + Cl^{\cdot} \qquad \text{R(S1)}$$

$$HO + HBr \rightarrow H_2O + Br^{\cdot} \qquad \text{R(S2)}$$

Thus, $Cl^{\cdot}$ and $Br^{\cdot}$ radical production rate P_{Cl} and P_{Br} can be calculated based on formula E(2) and E(3), respectively.

$$P_{Cl} = k_{Cl} \times [HCl] \times [OH] \qquad \text{E(2)}$$

$$P_{Br} = k_{Br} \times [HBr] \times [OH] \qquad \text{E(3)}$$

Where, rate coefficient $k_{Cl} = 1.7\times10^{-12}\times\exp(-230/T)$ cm^3 $molecule^{-1}$ s^{-1} over the temperature range 200-300 K and $k_{Br} = 6.7\times10^{-12}\times\exp(155/T)$ cm^3 $molecule^{-1}$ s^{-1} over the temperature range 180-370 K (http://iupac.pole-ether.fr.). [HCl] and [HBr] stand for HCl and HBr concentration.

References:

Benson, D.R., Young, L.H., Lee, S.H., Campos, T.L., Rogers, D.C., Jensen, J., 2008. The effects of airmass history on new particle formation in the free troposphere: case studies. Atmos. Chem. Phys. 8, 3015-3024.

Canagaratna, M.R., Jayne, J.T., Jimenez, J.L., Allan, J.D., Alfarra, M.R., Zhang, Q., Onasch, T.B., Drewnick, F., Coe, H., Middlebrook, A., Delia, A., Williams, L.R., Trimborn, A.M., Northway, M.J., DeCarlo, P.F., Kolb, C.E., Davidovits, P., Worsnop, D.R., 2007. Chemical and microphysical characterization of ambient aerosols with the aerodyne aerosol mass spectrometer. Mass Spectrom Rev 26, 185-222.

Drinovec, L., Močnik, G., Zotter, P., Prévôt, A.S.H., Ruckstuhl, C., Coz, E., Rupakheti, M., Sciare, J., Müller, T., Wiedensohler, A., 2014. The "dual-spot" Aethalometer: an improved measurement of aerosol black carbon with real-time loading compensation. Atmospheric Measurement Techniques 8, 1965-1979.

He, K.B., Yang, F.M., Ma, Y.L., Zhang, Q., Yao, X.H., Chan, C.K., Cadle, S., Chan, T., Mulawa, P., 2001. The characteristics of $PM_{2.5}$ in Beijing, China. Atmospheric Environment 35, 4959-4970.

Iyer, S., Lopez-Hilfiker, F., Lee, B., Thornton, J., Kurtén, T., 2016. Modeling the Detection of Organic and Inorganic Compounds Using Iodide-Based Chemical Ionization. The journal of physical chemistry. A 120.

Keuken, M.P., Schoonebeek, C.A.M., van Wensveen-Louter, A., Slanina, J., 1988. Simultaneous sampling of NH_3, HNO_3, HC1, SO_2 and H_2O_2 in ambient air by a wet annular denuder system. Atmospheric Environment (1967) 22, 2541-2548.

Liu, Y., Zhang, Y., Lian, C., Yan, C., Feng, Z., Zheng, F., Fan, X., Chen, Y., Wang, W., Chu, B., Wang, Y., Cai, J., Du, W., Daellenbach, K.R., Kangasluoma, J., Bianchi, F., Kujansuu, J., Petäjä, T., Wang, X., Hu, B., Wang, Y., Ge, M., He, H., Kulmala, M., 2020. The promotion effect of nitrous acid on aerosol formation in wintertime Beijing: possible contribution of traffic-related emission. Atmos. Chem. Phys. Discuss. 2020, 1-43.

Neese, F., 2012. The ORCA program system. Wiley Interdisciplinary Reviews: Computational Molecular Science 2, 73-78.

Otjes, R.P., Wyers, G.P., Slanina, J., 1993. A continuous-flow denuder for the measurement of ambient concentrations and surface-exchange fluxes of ammonia. Atmospheric Environment Part A General Topics 27, 2085-2090.

Riplinger, C., Neese, F., 2013. An efficient and near linear scaling pair natural orbital based local coupled cluster method. Journal of Chemical Physics 138, 064103.

Rumsey, I.C., Cowen, K.A., Kelly, T.J., Hanft, E.A., Walker, J.T., 2011. An assessment of the performance of the Monitor for AeRosols and GAses in ambient air (MARGA): A semi-continuous method for soluble compounds. Atmospheric Chemistry and Physics 14, 0327.

Tan, Z., Lu, K., Jiang, M., Su, R., Zhang, Y., 2019. Daytime atmospheric oxidation capacity in four Chinese megacities during the photochemically polluted season: A case study based on box model simulation. Atmospheric Chemistry and Physics 19, 3493-3513.

Wang, Z., Wu, Z., Yue, D., Shang, D., Guo, S., Sun, J., Ding, A., Wang, L., Jiang, J., Guo, H., Gao, J., Cheung, H.C., Morawska, L., Keywood, M., Hu, M., 2017. New particle formation in China: Current knowledge and further directions. Sci. Total Environ. 577, 258-266.

Wilson, A.K., Woon, D.E., Peterson, K.A., Dunning, T.H., 1999. Gaussian Basis Sets for Use in Correlated Molecular Calculations. IX. The Atoms Gallium Through Krypton. The Journal of Chemical Physics 110, 7667-7676.

Xu, Z., Wang, T., Wu, J., Xue, L., Chan, J., Zha, Q., Zhou, S., Louie, P.K.K., Luk, C.W.Y., 2015. Nitrous acid (HONO) in a polluted subtropical atmosphere: Seasonal variability, direct vehicle emissions and heterogeneous production at ground surface. Atmospheric Environment 106, 100-109.

Yu, H., Ren, L., Kanawade, V.P., 2017. New Particle Formation and Growth Mechanisms in Highly Polluted Environments. Current Pollution Reports 3, 10.1007/s40726-017-0067-3.

Yu, L., Wang, G., Zhang, R., Zhang, L., Song, Y., Wu, B., Li, X., An, K., Chu, J., 2013. Characterization and Source Apportionment of $PM_{2.5}$ in an Urban Environment in Beijing. Aerosol and Air Quality Research 13, 574-583.